Trinuclear Ruthenium Clusters as Bivalent Electrochemical Probes for Ligand-Receptor Binding Interactions

Daniel J. Feld, Hsiao-Tieh Hsu, Amanda L. Eckermann*, and Thomas J. Meade*

Departments of Chemistry, Molecular Biosciences, Neurobiology, Biomedical Engineering, & Radiology, Northwestern University, 2145 Sheridan Rd., Evanston, IL 60208, USA Email: a-eckermann@northwestern.edu, tmeade@northwestern.edu

SUPPORTING INFORMATION

EXPERIMENTAL

Syntheses

5-(2-Oxo-hexahydro-thieno[3,4-d]imidazol-4-yl)-pentanoic acid (pyridin-4-ylmethyl)-amide (4-BMP). 4-BMP was synthesized according to previously published methods.[1, 2] This compound was characterized by NMR and mass spectrometry.

16-Mercapto-*N*-(pyridine-4-ylmethyl)hexadecanamide (pyC16SH). 16-mercaptohexadecanoic acid (100 mg, 0.34 mmol), dicyclohexylcarbodiimide (75mg, 0.36 mmol), and 4-aminomethylpyridine (38 μL, 0.37 mmol) were dissolved in 10 mL of 4:1 CH_2Cl_2/acetone. This solution was allowed to stir overnight at room temperature during which time a white precipitate formed. The precipitate was removed by vacuum filtration using Whatman No. 1 filter paper. The filtrate was purified by column chromatography (silica, 5% MeOH/$CHCl_3$). The solvent was evaporated under reduced pressure to give the product as a white solid. Yield: 88%. ^{1}H NMR (500 MHz, $CDCl_3$) δ 8.57 (d, 2H), 7.20 (d, 2H), 4.46 (s, 2H), 2.51 (t, 2H), 2.23 (t, 2H), 1.69 (m, 4H), 1.60 (q, 2H), 1.4-1.2 (m, 20H). ^{13}C NMR (500 MHz, $CDCl_3$) δ 173.5, 150.0, 147.7, 122.3, 42.2, 36.6, 34.1, 29.6, 29.5, 29.3, 29.1, 28.5, 28.4, 25.8, 24.7. ESI-MS (*m/z*): Calcd. for (M + H): 379.2 Found 379.2.

$[Ru_3O(OAc)_6CO(MeOH)_2]^0$. (1) The procedure was carried out using a previously published method, starting with either $RuCl_3 \bullet xH_2O$ or hexaacetatotriaquaoxotriruthenium acetate.[3, 4] The product was characterized by ^{1}H NMR and UV-visible spectroscopy.

$[Ru_3O(OAc)_6CO(4\text{-}BMP)(MeOH)]^0$. (2) $[Ru_3O(OAc)_6CO(MeOH)_2]^0$ (77 mg, 0.10 mmol) was dissolved in 50 mL of 1:1 MeOH/CH_2Cl_2. To this solution was added 4-BMP (27 mg, 0.08 mmol). The resulting solution was stirred for 3 days at room temperature

and followed by TLC. During this time it turned bluish purple. The product was purified by column chromatography (silica, 10% MeOH/$CHCl_3$). The solvent was evaporated under reduced pressure to give the product as a bluish purple powder. Yield: 47%. ^{1}H NMR (500 MHz, MeOD) δ 8.95 (d, 2H), 7.98 (d, 2H), 4.82 (s, 2H), 4.38 (m, 1H), 4.20 (m, 1H), 3.13 (q, 2H), 2.82 (dd, 1H), 2.55 (dd, 1H) 2.35 (t, 4H), 1.85 (s, 6H), 1.80 (s, 6H), 1.75-1.50 (m, 10H), 1.50-1.35 (m, 2H) UV-visible (MeOH) λ_{max} = 568 nm.

$[Ru_3O(OAc)_6CO(4\text{-}BMP)(py)]^0$ (3). $[Ru_3O(OAc)_6CO(4\text{-}BMP)(MeOH)]^0$ (33 mg, 0.03 mmol) was dissolved in 10 mL of 1:1 MeOH/CH_2Cl_2. To this solution was added pyridine (75 μL, 0.92 mmol). The resulting solution was allowed to stir at room temperature overnight during which time it turned blue. Progression of the reaction was monitored by TLC. The product was purified by column chromatography (silica, 10% MeOH/$CHCl_3$). The solvent was evaporated under reduced pressure to give the product as a blue solid. Yield: 69%. ^{1}H NMR (500 MHz, MeOD) δ 9.05 (d, 2H), 8.98 (d, 2H), 8.25 (t, 1H), 8.11 (t, 2H), 7.99 (d, 2H) 4.87 (s, 2H), 4.41 (m, 1H), 4.25 (m, 1H), 3.22 (q, 1H), 2.87 (dd, 1H), 2.65 (dd, 1H) 2.40 (t, 2H), 1.94 (s, 12H), 1.78-1.53 (m, 10H), 1.53-1.47 (m, 2H) UV-visible (MeOH) λ_{max} = 584 nm.

$[Ru_3O(OAc)_6CO(4\text{-}BMP)_2]^0$ (4). $[Ru_3O(OAc)_6CO(MeOH)_2]^0$ (101 mg, 0.13 mmol) was dissolved in 10 mL of 1:1 MeOH/CH_2Cl_2. To this solution was added 4-BMP (97 mg, 0.29 mmol). The resulting solution was allowed to stir overnight at room temperature during which time the reaction turned blue. Progression of the reaction was monitored by TLC. The product was purified by column chromatography (silica, 10% MeOH/$CHCl_3$). The solvent was evaporated under reduced pressure to give the product as a blue solid. Yield: 74%. ^{1}H NMR (500 MHz, MeOD) δ 9.11 (d, 2H), 8.08 (d, 2H),

4.95 (s, 2H), 3.80 (m, 1H), 3.70 (m, 1H), 2.43 (t, 2H), 1.96 (s, 6H), 1.90 (s, 6H), 1.83-1.74 (m, 8H), 1.58-1.4 (m, 6H), 1.10 (d, 3H) ^{13}C NMR (500 MHz, MeOD) δ 193.5, 193.2, 176.6, 154.7, 152.5, 124.0, 63.4, 61.6, 57.2, 43.0, 41.1, 36.8, 30.0, 29.6, 26.9, 23.7, 22.0. UV-visible (MeOH) λ_{max} = 582 nm.

$[Ru_3O(OAc)_6CO(py)(MeOH)]^0$. (5). $[Ru_3O(OAc)_6CO(py)(MeOH)]^0$ was synthesized according to previously published methods.[4] This compound was characterized by NMR and UV-visible spectroscopy.

$[Ru_3O(OAc)_6CO(4\text{-}BMP)(pyC16SH)]^0$. (6) $[Ru_3O(OAc)_6CO(4\text{-}BMP)(MeOH)]^0$ (68 mg, 0.06 mmol) was dissolved in 10 mL of 1:1 MeOH/CH_2Cl_2. To this solution was added pyC16SH (84 mg, 0.27 mmol). The resulting solution was stirred at room temperature overnight during which time it turned blue Progression of the reaction was monitored by TLC. The product was purified by column chromatography (silica, 10% MeOH/$CHCl_3$). The solvent was evaporated under reduced pressure to give the product as a blue solid. Yield: 80%. ^{1}H NMR (500 MHz, MeOD) δ 8.93 (d, 2H), 7.98 (s, 2H), 4.85 (s, 1H), 4.38 (m, 1H), 4.22 (m, 1H), 3.13 (q, 1H), 2.82 (dd, 1H), 2.55-2.50 (m, 3H), 2.38-2.23 (m, 4H), 1.86 (s, 12H), 1.75-1.48 (m, 16H), 1.48-1.38 (m, 4H), 1.36-1.10 (m, 22H) UV-visible (MeOH) λ_{max} = 585 nm.

$[Ru_3O(OAc)_6CO(py)(pyC16SH)]^0$. (7) $[Ru_3O(OAc)_6CO(py)(MeOH)]^0$ (92 mg, 0.11 mmol) was dissolved in 10 mL of 1:1 MeOH/CH_2Cl_2. To this solution was added pyC16SH (90 mg, 0.24 mmol). The resulting solution was stirred overnight at room temperature and followed by TLC. During this time it turned blue. The product was purified by column chromatography (silica, 5% MeOH/$CHCl_3$). The solvent was evaporated under reduced pressure to give the product as a blue solid. Yield: 45%. ^{1}H

NMR (500 MHz, $CDCl_3$) δ 9.10 (d, 2H), 9.00 (d, 2H), 8.19 (t, 1H), 8.04 (t, 2H), 7.92 (d, 2H), 4.91 (s, 2H), 2.49 (t, 2H), 2.38 (t, 2H), 2.09 (s, 12H), 1.81 (s, 6H), 1.75 (m, 2H), 1.63 (m, br, 4H), 1.4-1.1 (m 20H) UV-visible (MeOH) λ_{max} = 582 nm.

HABA/avidin assays

HABA/avidin reagent was purchased from Sigma and was reconstituted with 10 mL water. The assay was conducted according to the instructions provided by Sigma. In a typical experiment 10 μL aliquots of 0.08 mM sample in water were titrated into 450 μL of the reconstituted HABA/avidin solution. The decrease in absorbance at 500 nm (ΔA_{500}) due to the release of HABA from the avidin binding pocket was monitored using UV-visible spectroscopy. Due to the nonzero absorbance at 500 nm of **3** and **4**, the titrations were additionally performed in water (no HABA/avidin) so this absorbance could be subtracted from the HABA/avidin data. Equation 3 was used to calculate each ΔA_{500} plotted in the absorption titration curves. In this equation, V_0 is the initial volume of HABA/avidin solution, V_i is the total volume of sample solution added, $A_{HABA+sample}$ is the absorbance at 500 nm after addition of each aliquot to HABA/avidin, A_{sample} is the absorbance at 500 nm of sample during the titration in water, and A_{HABA} is the initial absorbance at 500 nm of the HABA/avidin solution. Absorption titration curves plotting $-\Delta A_{500}$ vs [complex]:[avidin] were used to determine the equivalence point in each titration.

$$\Delta A_{500} = \left[\frac{V_0}{V_0 + V_i} \left(A_{HABA+sample} \right) + A_{sample} \right] - A_{HABA} \qquad (1)$$

FIGURES

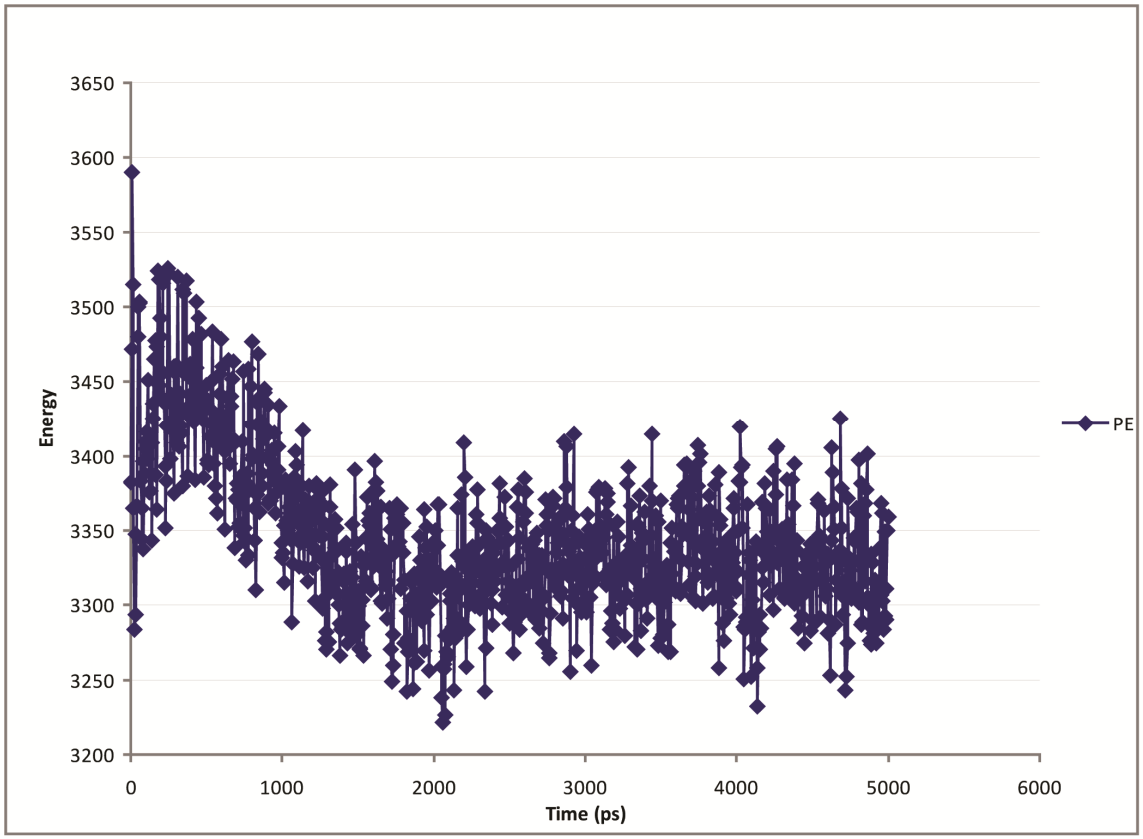

Figure S1: Time versus energy plot showing the equilibrium condition at 5 ns of **4** bound to avidin. A minimum energy configuration was reached in approximately 2 ns. In this minimum energy configuration all expected interactions between the biotin binding ligands and avidin are maintained.

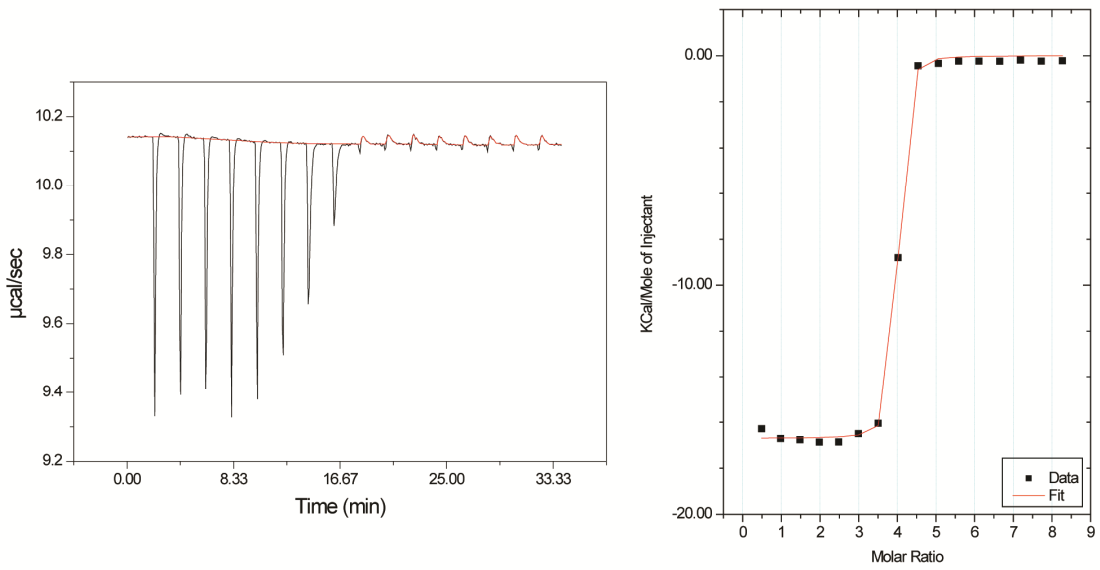

Figure S2: Isothermal titration calorimetry data for 4-BMP. The left plot is the raw ITC data for the titration of 4-BMP into a solution of avidin. The right shows the heat of reaction plotted vs. the ratio of metal complex titrated into the solution relative to protein.

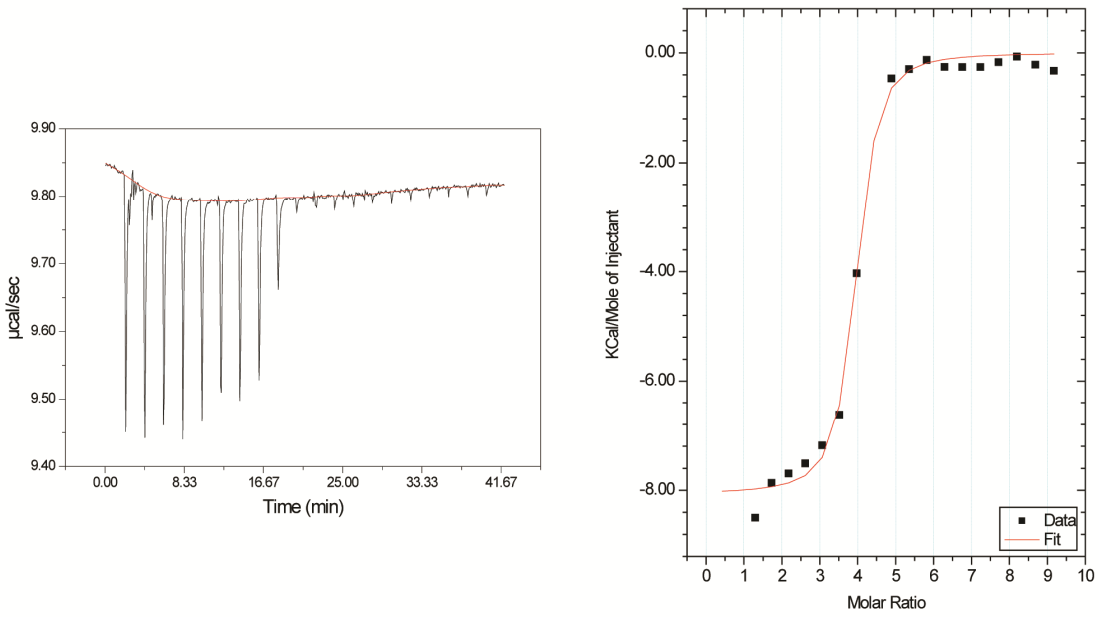

Figure S3: Isothermal titration calorimetry data for **3**. The left plot is the raw ITC data for the titration of **3** into a solution of avidin. The right shows the heat of reaction plotted vs. the ratio of metal complex titrated into the solution relative to protein.

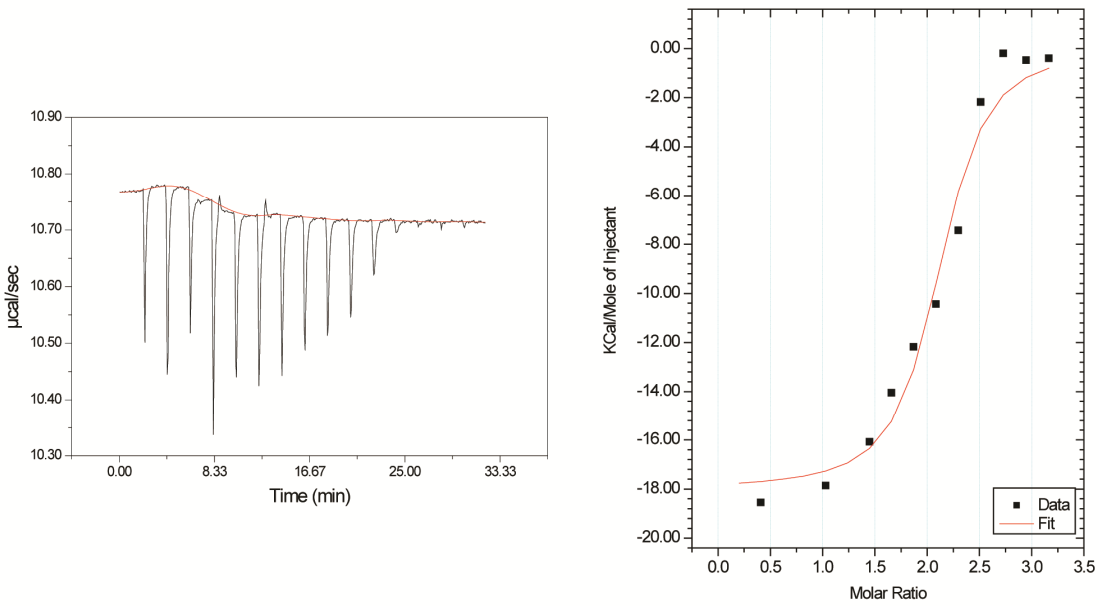

Figure S4: Isothermal titration calorimetry data for **4**. The left plot is the raw ITC data for the titration of **4** into a solution of avidin. The right shows the heat of reaction plotted vs. the ratio of metal complex titrated into the solution relative to protein.

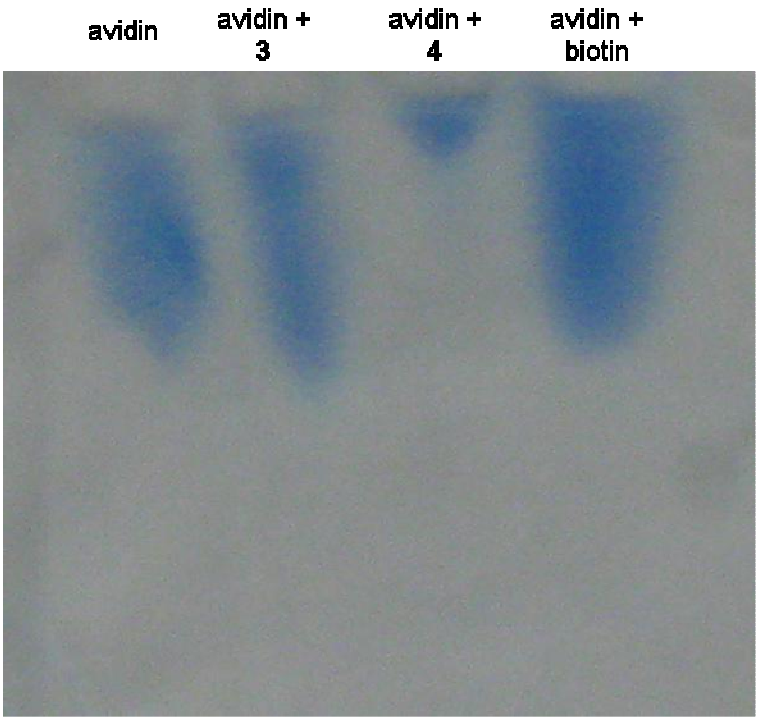

Figure S5: Native gel showing the migration of native avidin, avidin + **3**, avidin + **4**, and avidin + biotin. Protein binding ligands were allowed to bind to avidin at room temperature overnight. Avidin + **4** was observed to migrate more slowly than native avidin, avidin + **3**, and avidin + biotin. The slower migration is due to a larger molecular weight conjugate, indicating that the bivalent cluster **4** links multiple proteins together. For the bivalent cluster **4** in solution, intermolecular protein binding is occurring.

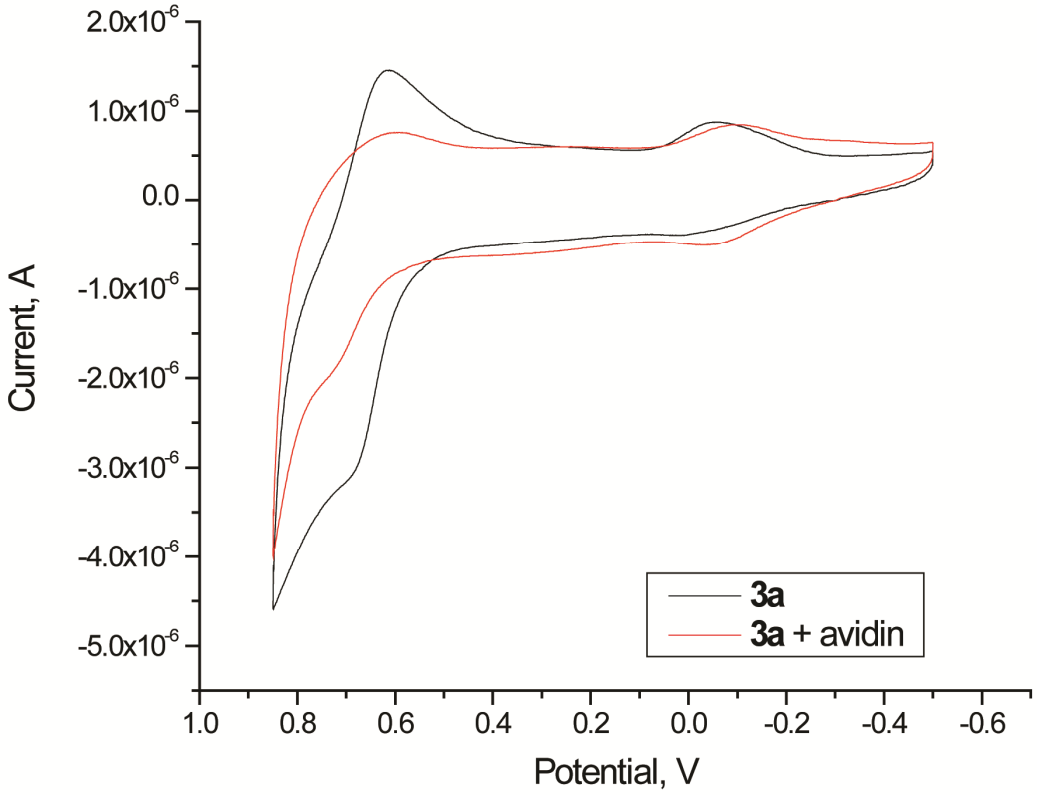

Figure S6: Solution CV data (vs. Ag/AgCl) for **3a** (black). Upon oxidation, the carbonyl is lost from **3** ($E_{1/2}$ ~ 650 mV) and the corresponding aquo species, **3a** is formed, ($E_{1/2}$ ~ -50 mV). Upon avidin addition (red), a shift in $E_{1/2}$ of -58 mV is observed.

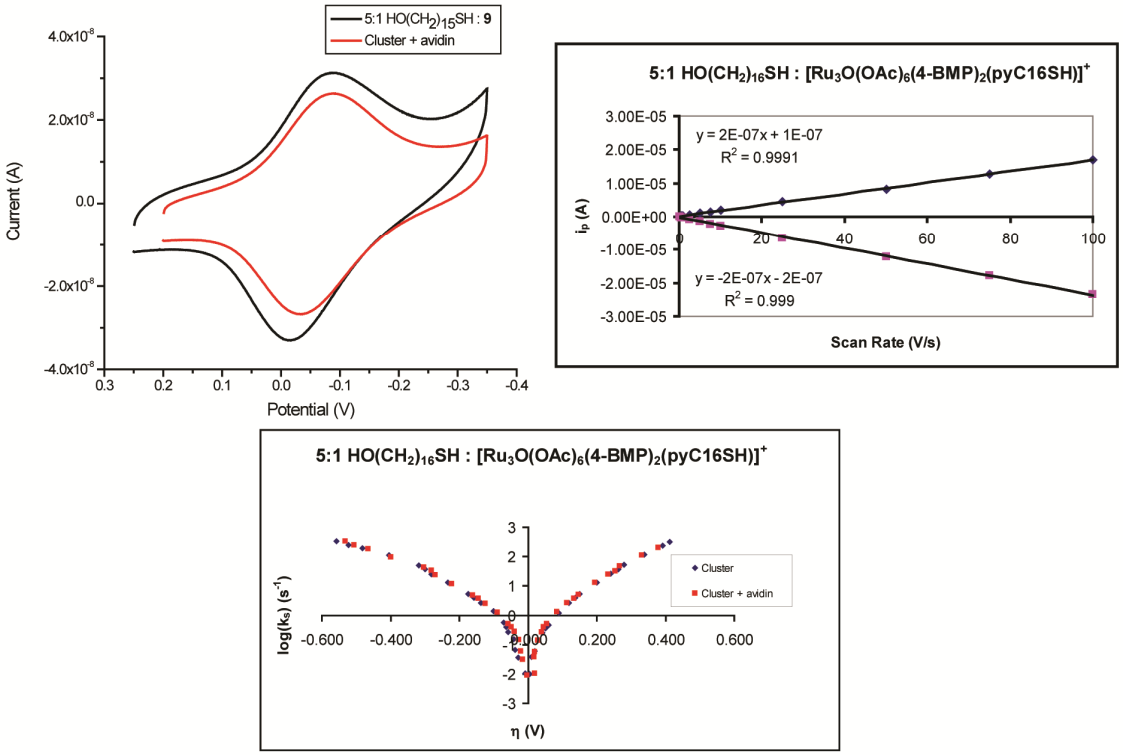

Figure S7: (top left) CV (vs. Ag/AgCl) of 5:1 diluent $HO(CH_2)_{16}SH$ to **9**. A shift of -11 mV from the original monolayer (black line) after avidin addition (red line) was observed. (top right) A plot of peak current vs. scan rate for the monolayer was linear. A linear relationship indicates a well-formed monolayer, free from diffusion effects. (bottom) Tafel plot of electrochemistry of 5:1 $HO(CH_2)_{16}SH$/**9** (blue diamonds), cluster after 30 μM avidin soak overnight at 37 °C (orange squares). k_{ET} of approximately 0.3 s^{-1} was observed. Upon avidin addition, negligible change in the y-intercept (k_0) and curvature (λ) was observed.

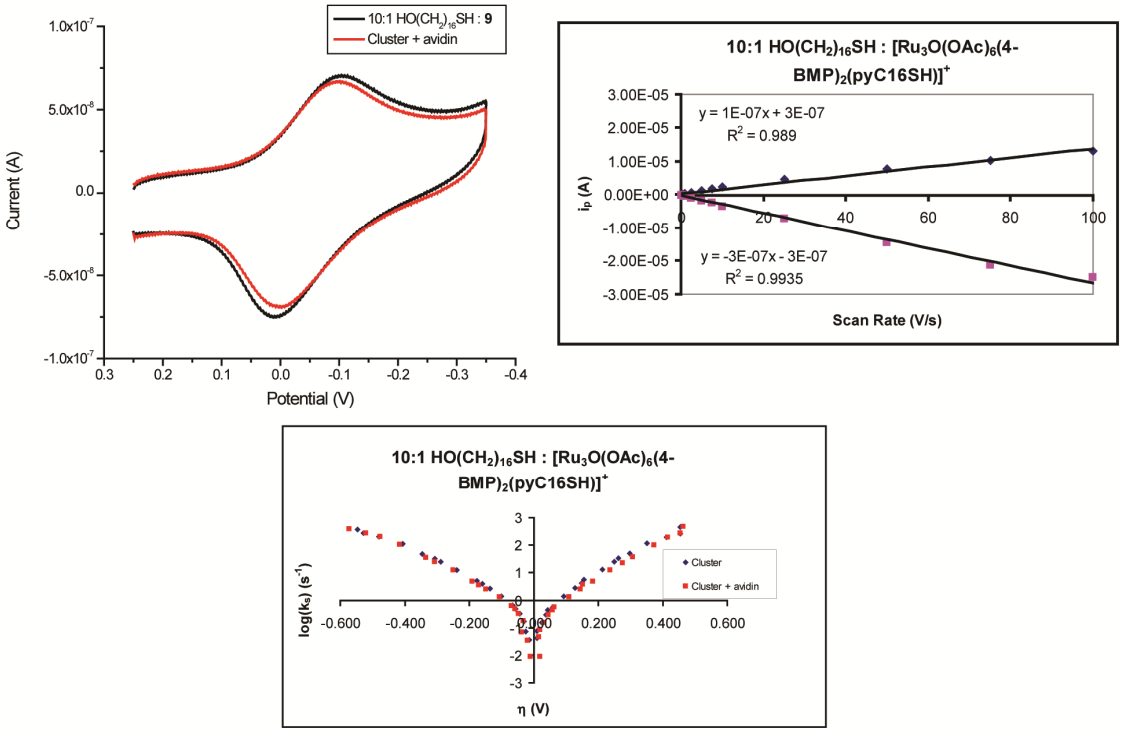

Figure S8: (top left) CV (vs. Ag/AgCl) of 10:1 diluent $HO(CH_2)_{16}SH$ to **9**. No shift in $E_{1/2}$ from the original monolayer (black line) after avidin addition (red line) was observed. (top right) A plot of peak current vs. scan rate for the monolayer was linear. A linear relationship indicates a well-formed monolayer, free from diffusion effects. (bottom) Tafel plot of electrochemistry of 10:1 $HO(CH_2)_{16}SH$/**9** (blue diamonds), cluster after 30 μM avidin soak overnight at 37 °C (orange squares). k_{ET} of approximately 0.3 s^{-1} was observed. Upon avidin addition, negligible change in the y-intercept (k_0) and curvature (λ) was observed.

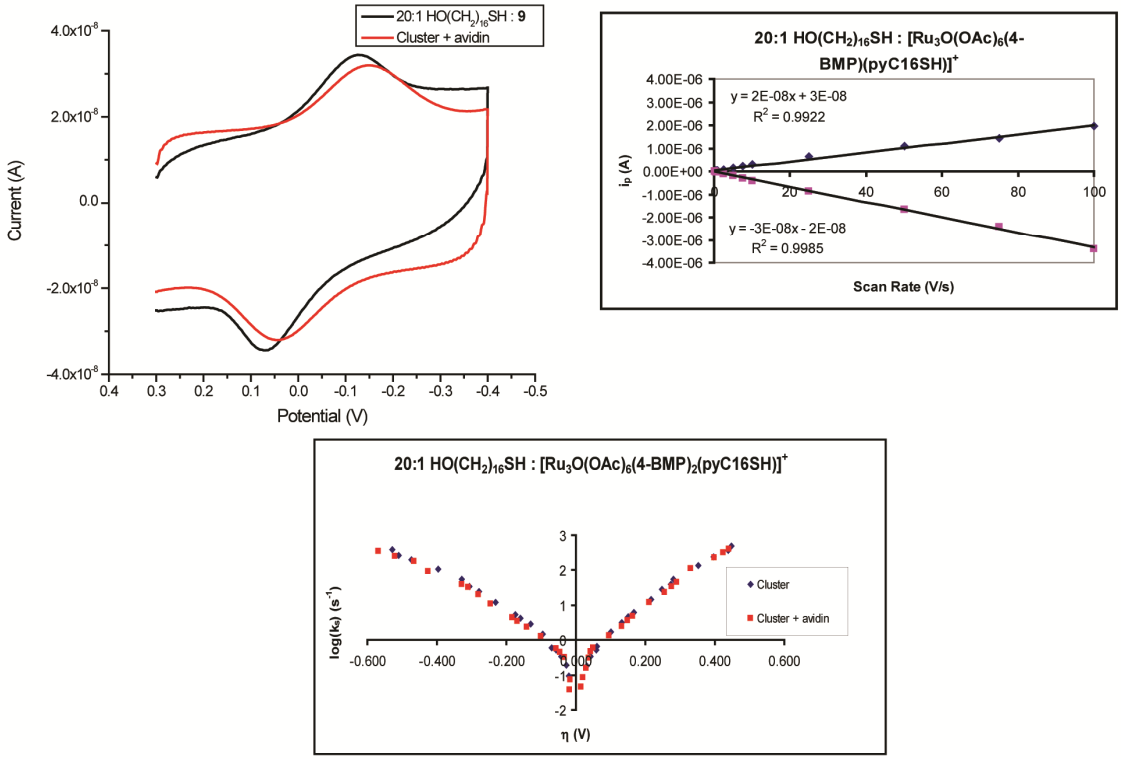

Figure S9: (top left) CV (vs. Ag/AgCl) of 20:1 diluent $HO(CH_2)_{16}SH$ to **9**. A shift of -23 mV from the original monolayer (black line) after avidin addition (red line) was observed. (top right) A plot of peak current vs. scan rate for the monolayer was linear. A linear relationship indicates a well-formed monolayer, free from diffusion effects. (bottom) Tafel plot of electrochemistry of 20:1 $HO(CH_2)_{16}SH$/**9** (blue diamonds), cluster after 30 μM avidin soak overnight at 37 °C (orange squares). k_{ET} of approximately 0.4 s^{-1} was observed. Upon avidin addition, negligible change in the y-intercept (k_0) and curvature (λ) was observed.

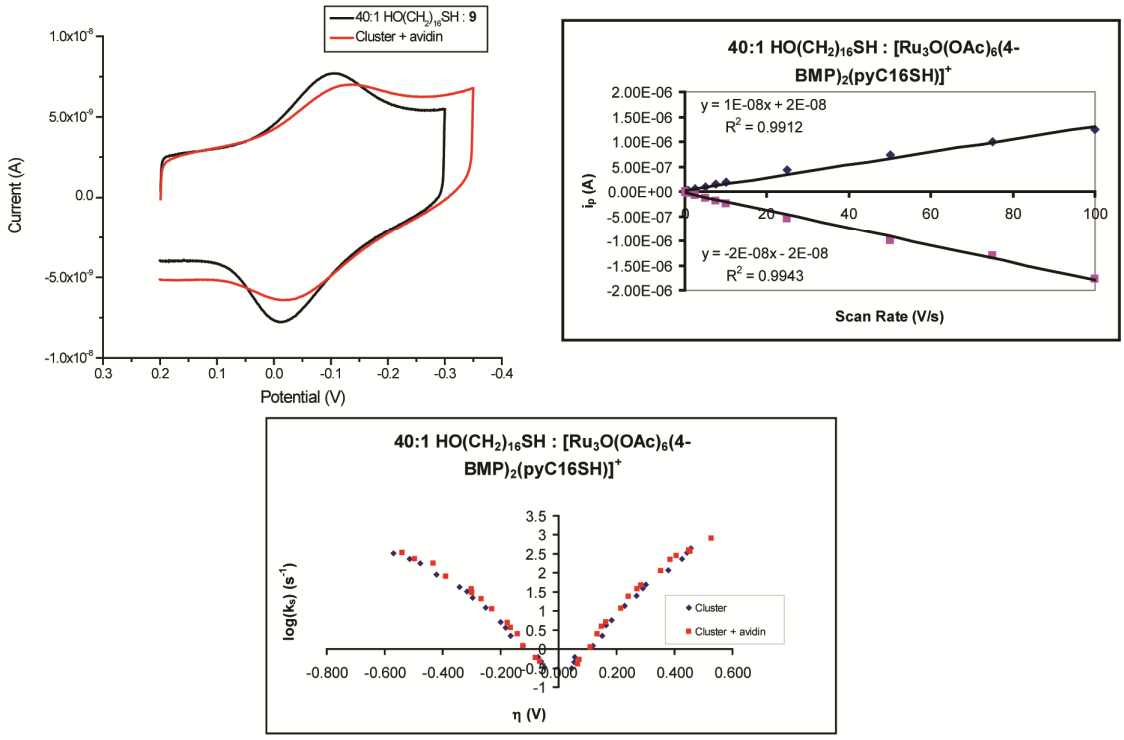

Figure S10: (top left) CV (vs. Ag/AgCl) of 40:1 diluent $HO(CH_2)_{16}SH$ to **9**. A shift of -23 mV from the original monolayer (black line) after avidin addition (red line) was observed. (top right) A plot of peak current vs. scan rate for the monolayer was linear. A linear relationship indicates a well-formed monolayer, free from diffusion effects. (bottom) Tafel plot of electrochemistry of 40:1 $HO(CH_2)_{16}SH$/**9** (blue diamonds), cluster after 30 μM avidin soak overnight at 37 °C (orange squares). k_{ET} of approximately 0.3 s^{-1} was observed. Upon avidin addition, negligible change in the y-intercept (k_0) and curvature (λ) was observed.

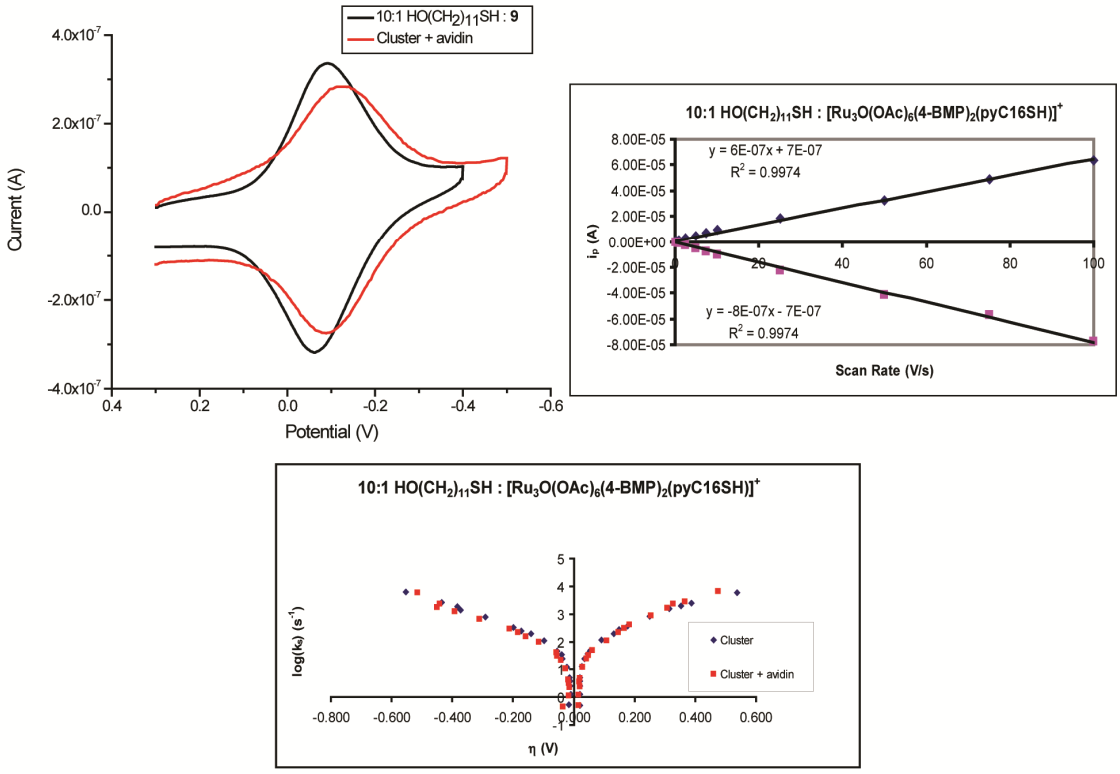

Figure S11: (top left) CV (vs. Ag/AgCl) of 10:1 diluent $HO(CH_2)_{11}SH$ to **9**. A shift of -28 mV from the original monolayer (black line) after avidin addition (red line) was observed. (top right) A plot of peak current vs. scan rate for the monolayer was linear. A linear relationship indicates a well-formed monolayer, free from diffusion effects. (bottom) Tafel plot of electrochemistry of 10:1 $HO(CH_2)_{11}SH$/**9** (blue diamonds), cluster after 30 μM avidin soak overnight at 37 °C (orange squares). k_{ET} of approximately 60 s^{-1} was observed. Upon avidin addition, negligible change in the y-intercept (k_0) and curvature (λ) was observed.

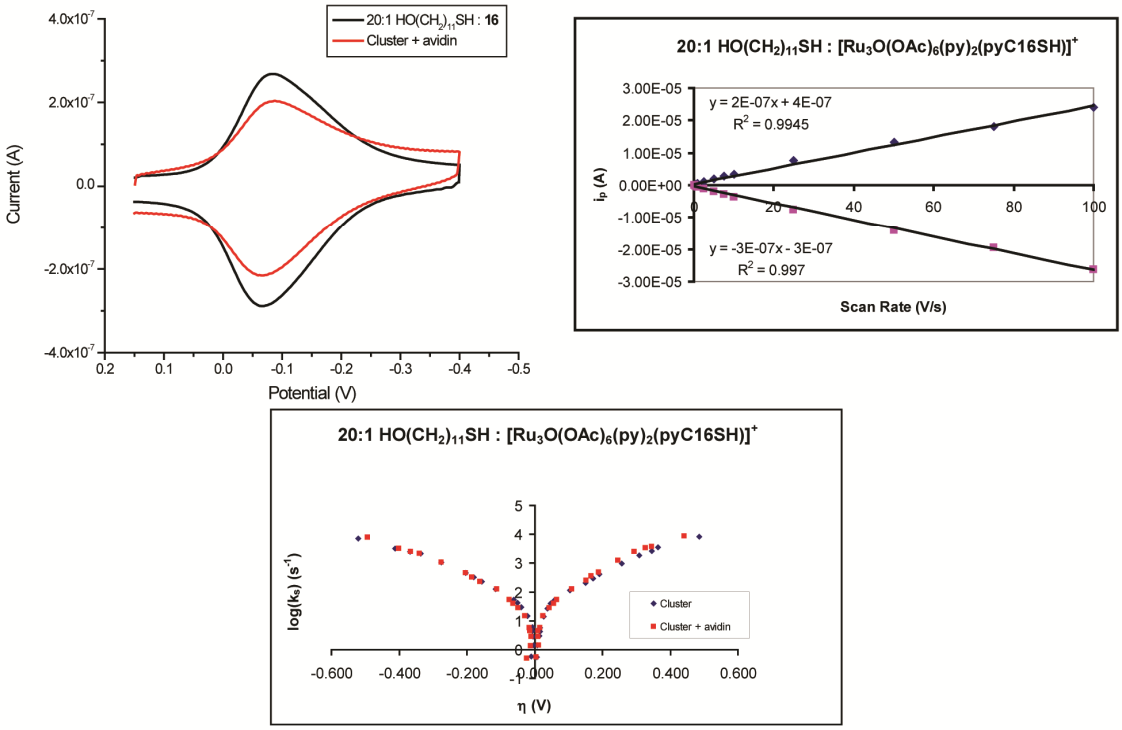

Figure S12: (top left) CV (vs. Ag/AgCl) of 20:1 diluent $HO(CH_2)_{11}SH$ to **10**. No shift in $E_{1/2}$ from the original monolayer (black line) after avidin addition (red line) was observed. The decrease in peak current is likely due to nonspecific binding of avidin. (top right) A plot of peak current vs. scan rate for the monolayer was linear. A linear relationship indicates a well-formed monolayer, free from diffusion effects. (bottom) Tafel plot of electrochemistry of 20:1 $HO(CH_2)_{11}SH$/**10** (blue diamonds), cluster after 30 μM avidin soak overnight at 37 °C (orange squares). k_{ET} of approximately 60 s^{-1} was observed. Upon avidin addition, negligible change in the y-intercept (k_0) and curvature (λ) was observed.

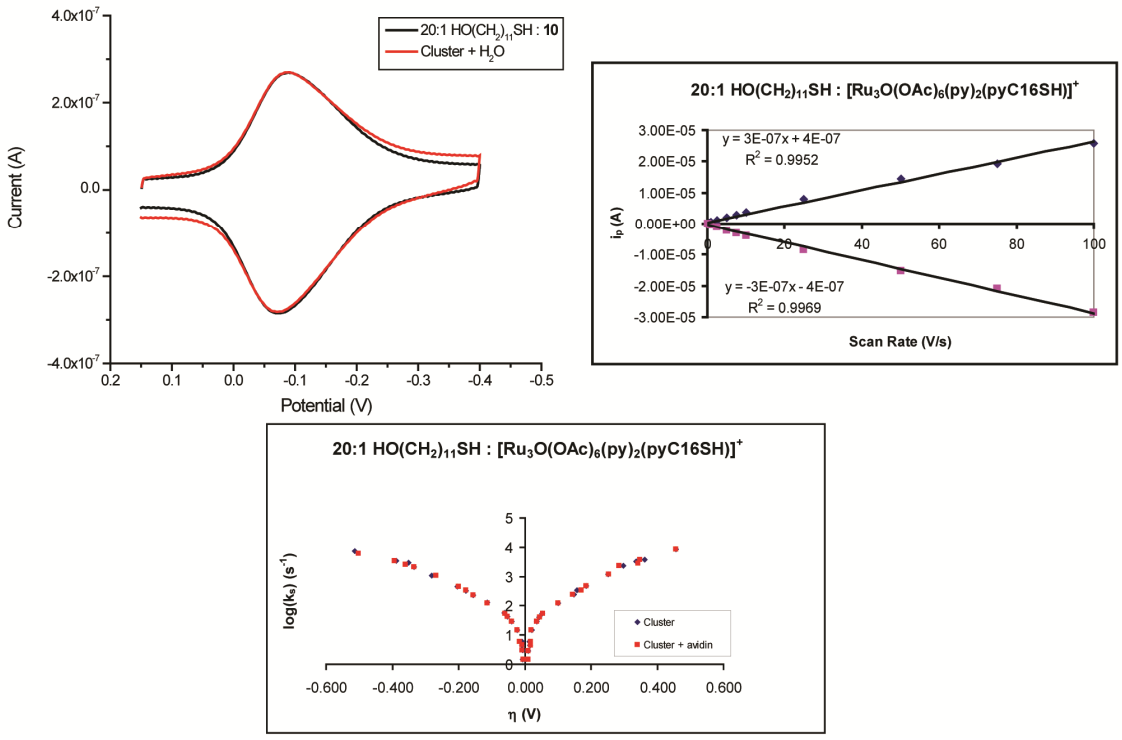

Figure S13: (top left) CV (vs. Ag/AgCl) of 20:1 diluent $HO(CH_2)_{11}SH$ to **10**. No shift in $E_{1/2}$ from the original monolayer (black line) after avidin addition (red line) was observed. The lack of a current decrease is evidence for nonspecific binding of avidin being the cause of the decrease in current observed for other systems studied. (top right) A plot of peak current vs. scan rate for the monolayer was linear. A linear relationship indicates a well-formed monolayer, free from diffusion effects. (bottom) Tafel plot of electrochemistry of 20:1 $HO(CH_2)_{11}SH$/**10** (blue diamonds), cluster after 30 μM avidin soak overnight at 37 °C (orange squares). k_{ET} of approximately 60 s^{-1} was observed. Upon avidin addition, negligible change in the y-intercept (k_0) and curvature (λ) was observed.

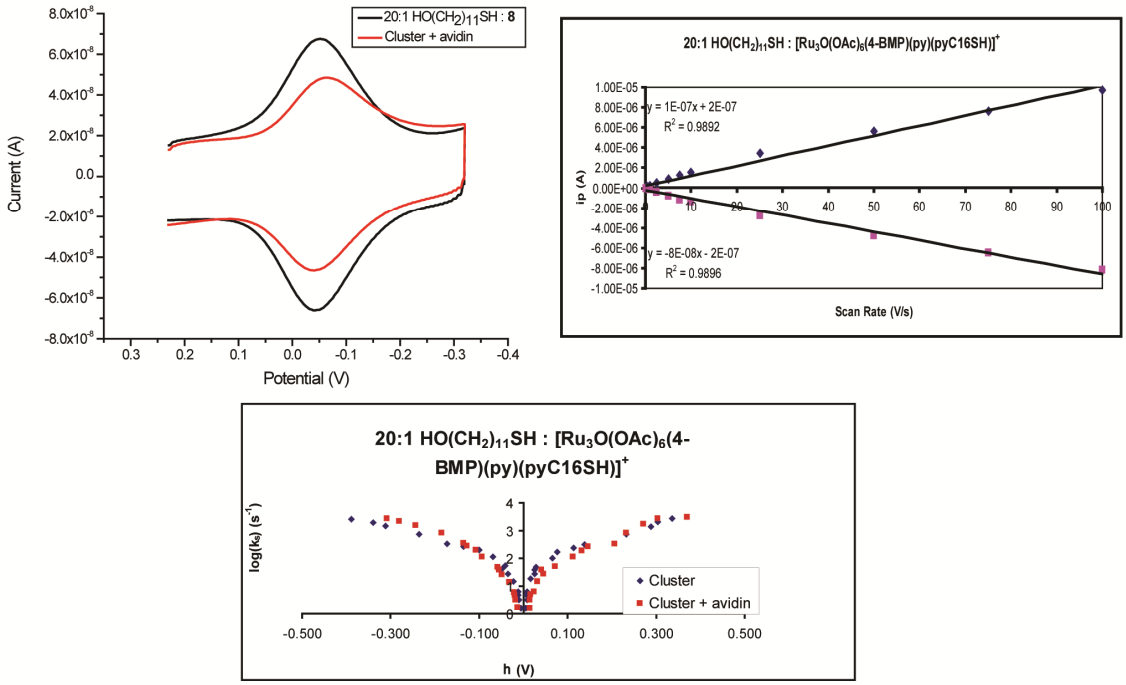

Figure S14: (top left) CV (vs. Ag/AgCl) of 20:1 diluent $HO(CH_2)_{11}SH$ to **8**. A shift of -6 mV from the original monolayer (black line) after avidin addition (red line) was observed. (top right) A plot of peak current vs. scan rate for the monolayer was linear. A linear relationship indicates a well-formed monolayer, free from diffusion effects. (bottom) Tafel plot of electrochemistry of 20:1 $HO(CH_2)_{11}SH$/**8** (blue diamonds), cluster after 30 μM avidin soak overnight at 37 °C (orange squares). k_{ET} of approximately 60 s^{-1} was observed. Upon avidin addition, negligible change in the y-intercept (k_0) and curvature (λ) was observed.

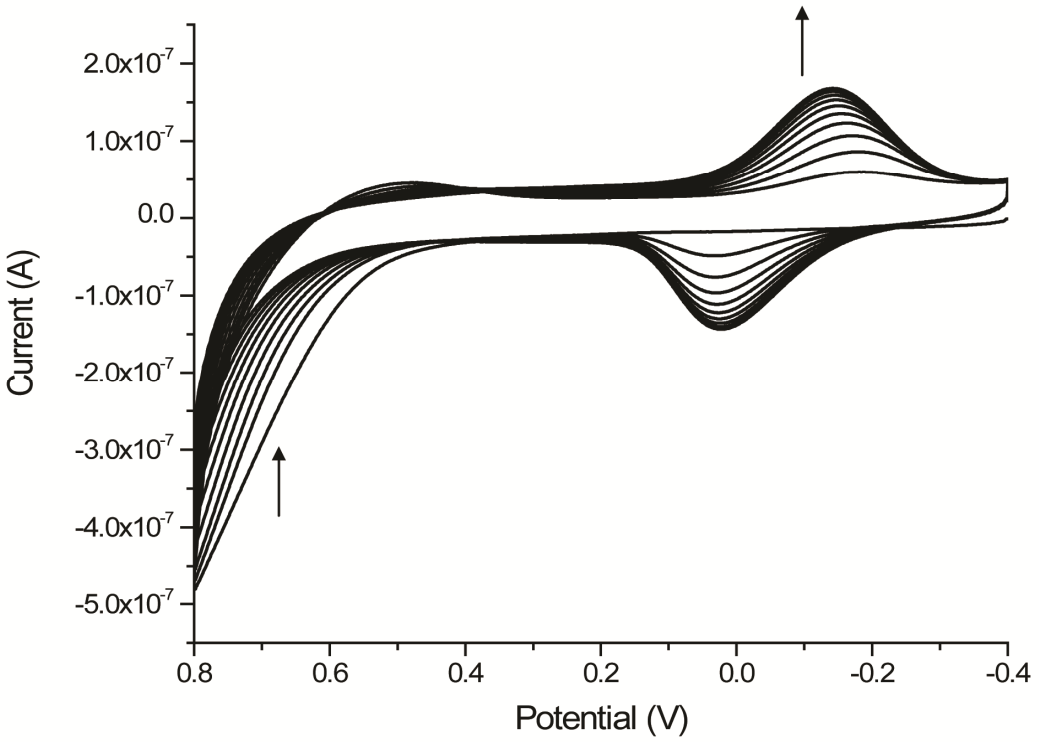

Figure S15: Cyclic voltammogram taken at a scan rate of 200 mV/s depicting electrochemical oxidation of **6** to form **6a**. As the potential is cycled, the peak with $E_{1/2}$ ~650 mV decreases as the CO becomes labile upon oxidation of the cluster. The peak for **6a** at lower potential is observed to increase as this complex is formed.

REFERENCES

(1) Eckermann, A. L.; Barker, K. D.; Hartings, M. R.; Ratner, M. A.; Meade, T. J., *J. Am. Chem. Soc.* **2005,** 127, (34), 11880-11881.
(2) Bannwarth, W.; Knorr, R., *Tetrahedron Lett.* **1991,** 32, (9), 1157-60.
(3) Goeltz, J. C.; Glover, S. D.; Hauk, J.; Kubiak, C. P.; Putman, R. D.; Rauchfuss, T. B., *Inorg. Synth.* **2010,** 35, 156-160.
(4) Baumann, J. A.; Salmon, D. J.; Wilson, S. T.; Meyer, T. J.; Hatfield, W. E., *Inorg. Chem.* **1978,** 17, (12), 3342-50.